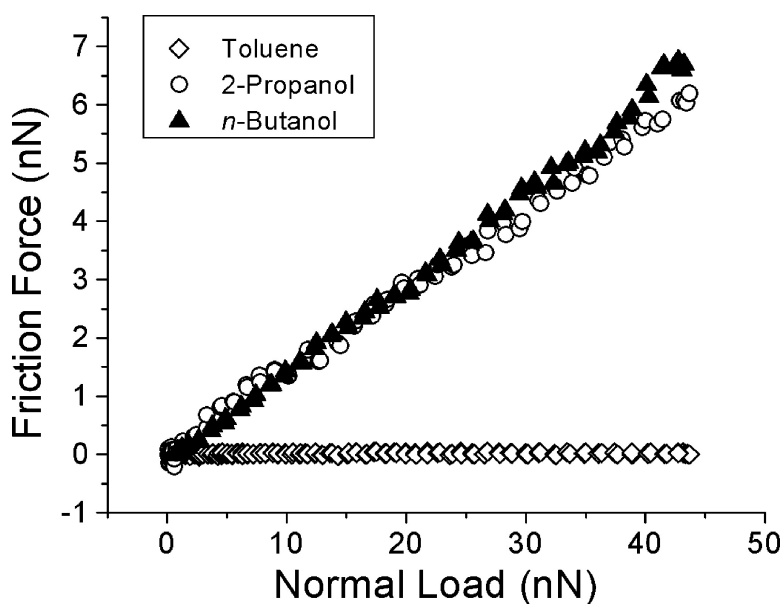


## Solvent Dependent Friction Force Response of Polystyrene Brushes Prepared by Surface Initiated Polymerization

F. T. Limpoco, Rigoberto C. Advincula, and Scott S. Perry

*Langmuir*, 2007, 23 (24), 12196-12201 • DOI: 10.1021/la701272a

Downloaded from <http://pubs.acs.org> on December 16, 2008



### More About This Article

Additional resources and features associated with this article are available within the HTML version:

- Supporting Information
- Links to the 4 articles that cite this article, as of the time of this article download
- Access to high resolution figures
- Links to articles and content related to this article
- Copyright permission to reproduce figures and/or text from this article

[View the Full Text HTML](#)



# Solvent Dependent Friction Force Response of Polystyrene Brushes Prepared by Surface Initiated Polymerization

F. T. Limpoco,<sup>†</sup> Rigoberto C. Advincula,<sup>‡</sup> and Scott S. Perry<sup>\*,§</sup>

Department of Chemistry, University of Florida, Gainesville, Florida 32611-7200,  
Department of Materials Science & Engineering, University of Florida, Gainesville, Florida 32611-6400,  
and Department of Chemistry, University of Houston, Houston, Texas 77204-5003

Received May 1, 2007. In Final Form: August 20, 2007

Polystyrene (PS) brushes were prepared on oxide passivated silicon by the surface initiated polymerization (SIP) technique. From an AIBN-type free radical initiator, which was silanized and immobilized on silicon wafers, styrene brushes were directly polymerized and grafted from the surface. The formation of the initiator monolayer and, subsequently, the polymer brush on the surface were monitored by X-ray photoelectron spectroscopy (XPS) and ellipsometry. Friction force measurements were performed by atomic force microscopy (AFM), using a 5  $\mu\text{m}$  SiO<sub>2</sub> colloidal sphere tip and under systematically varied solvent environments (nonpolar to polar), to demonstrate the dependence of brush lubricity on solvation. The relative uptake of solvents in the PS brush was determined by quartz crystal microbalance (QCM), and it correlates well with friction data. It is surmised that, in poor solvent environments, the polymer brush exists in a collapsed conformation, giving rise to the higher observed friction response.

## 1. Introduction

Surfaces modified with physically and chemically grafted polymer brushes are predicted to exhibit novel properties in terms of their adhesion, lubrication, viscoelasticity, and wettability.<sup>1–7</sup> Moreover, complex architectures can be achieved which lead to exquisitely tailored surfaces that are responsive to their environment,<sup>8,9</sup> including solvent switchable diblock<sup>10–15</sup> and mixed brushes,<sup>16–25</sup> nanopatterned brushes from lithographic

techniques,<sup>26–30</sup> vertically segregated brushes,<sup>31,32</sup> Y-shaped amphiphilic brushes,<sup>33,34</sup> and surface-attached dendrimers with tunable interfacial friction properties.<sup>35</sup>

This ability to modify surfaces with polymers is especially important in the regime of boundary lubrication where solid–solid contact occurs, and thus, there is generally greater friction and wear.<sup>36</sup> As lubricant thickness decreases to molecularly thin films, its physicochemical properties become more important than its bulk viscosity. Polymers densely tethered on surfaces are predicted to be highly stretched in a good solvent, and they have been considered as novel boundary layer lubricants.<sup>37,38</sup> In such systems, strong compression would tend to increase osmotic pressure within the brush, resulting in a tendency for the chains to swell back and expand, effectively manifesting repulsive interaction and low friction.<sup>39,40</sup>

\* To whom correspondence should be addressed.

<sup>†</sup> Department of Chemistry, University of Florida.

<sup>‡</sup> Department of Chemistry, University of Houston.

<sup>§</sup> Department of Materials Science & Engineering, University of Florida.

(1) *Polymer Brushes: Synthesis, Characterization, Application*; Advincula, R. C., Brittain, W. J., Caster, K. C., Rühle, J., Eds.; Wiley-VCH: Weinheim, 2004.

(2) Kreer, T.; Binder, K. *Langmuir* **2003**, *19*, 7551.

(3) Mansky, P.; Lin, Y.; Huang, E.; Russel, T. P.; Hawker, C. *Science* **1997**, *275*, 1458.

(4) Grest, G. S. *Phys. Rev. Lett.* **1996**, *76*, 4979.

(5) Klein, J. *Annu. Rev. Mater. Sci.* **1996**, *26*, 581.

(6) Klein, J.; Kumacheva, E.; Perahia, D.; Mahalu, D.; Warburg, S. *Faraday Discuss.* **1994**, *98*, 173.

(7) Halperin, A.; Tirrell, M.; Lodge, T. P. *Adv. Polym. Sci.* **1992**, *100*, 31.

(8) Minko, S. *J. Macromol. Sci., Polym. Rev.* **2006**, *46*, 397.

(9) Uhlmann, P.; Ionov, L.; Houbenov, N.; Nitschke, M.; Grundke, K.; Motornov, M.; Minko, S.; Stamm, M. *Prog. Org. Coat.* **2006**, *55*, 168.

(10) Ayres, N.; Cyrus, C. D.; Brittain, W. J. *Langmuir* **2007**, *23*, 3744.

(11) Brittain, W. J.; Boyes, S. G.; Granville, A. M.; Baum, M.; Mirov, B. K.; Akgun, B.; Zhao, B.; Blickle, C.; Foster, M. D. *Adv. Polym. Sci.* **2006**, *198*, 125.

(12) Boyes, S. G.; Granville, A. M.; Baum, M.; Akgun, B.; Mirov, B. K.; Brittain, W. J. *Surf. Sci.* **2004**, *570*, 1.

(13) Granville, A. M.; Boyes, S. G.; Akgun, B.; Foster, M. D.; Brittain, W. J. *Macromolecules* **2004**, *37*, 2790.

(14) Zhao, B.; Brittain, W. J.; Zhou, W.; Cheng, S. Z. D. *Macromolecules* **2000**, *33*, 8821.

(15) Zhao, B.; Brittain, W. J. *Macromolecules* **2000**, *33*, 8813.

(16) Motornov, M.; Sheparovych, R.; Tokarev, I.; Roiter, Y.; Minko, S. *Langmuir* **2007**, *23*, 13.

(17) LeMieux, M. C.; Julthongpipit, D.; Bergman, K. N.; Cuong, P. D.; Ahn, H.; Lin, Y.; Tsukruk, V. V. *Langmuir* **2004**, *20*, 10046.

(18) Draper, J.; Luzinov, I.; Minko, S.; Tokarev, I.; Stamm, M. *Langmuir* **2004**, *20*, 4064.

(19) Ionov, L.; Houbenov, N.; Sidorenko, A.; Stamm, M.; Luzinov, I.; Minko, S. *Langmuir* **2004**, *20*, 9916.

(20) Ionov, L.; Sidorenko, A.; Stamm, M.; Minko, S.; Zdyrko, B.; Klep, V.; Luzinov, I. *Macromolecules* **2004**, *37*, 7421.

(21) Lemieux, M.; Usov, D.; Minko, S.; Stamm, M.; Shulha, H.; Tsukruk, V. V. *Macromolecules* **2003**, *36*, 7244.

(22) Houbenov, N.; Minko, S.; Stamm, M. *Macromolecules* **2003**, *36*, 5897.

(23) Minko, S.; Luzinov, I.; Luchnikov, V.; Müller, M.; Patil, S.; Stamm, M. *Macromolecules* **2003**, *36*, 7268.

(24) Motornov, M.; Minko, S.; Eichhorn, K.; Nitschke, M.; Simon, F.; Stamm, M. *Langmuir* **2003**, *19*, 8077.

(25) Minko, S.; Müller, M.; Usov, D.; Scholl, A.; Froeck, C.; Stamm, M. *Phys. Rev. Lett.* **2002**, *88*, 035502-1.

(26) Lee, W.; Caster, K. C.; Kim, J.; Zauscher, S. *Small* **2006**, *2*, 848.

(27) Kaholek, M.; Lee, W.; Feng, J.; LaMattina, B.; Dyer, D.; Zauscher, S. *Chem. Mater.* **2006**, *18*, 3660.

(28) Kaholek, M.; Lee, W.; LaMattina, B.; Caster, K. C.; Zauscher, S. *Nano Lett.* **2004**, *4*, 373.

(29) Kaholek, M.; Lee, W.; Ahn, S.; Ma, H.; Caster, K. C.; LaMattina, B.; Zauscher, S. *Chem. Mater.* **2004**, *16*, 3688.

(30) Ionov, L.; Minko, S.; Stamm, M.; Gohy, J.; Jérôme, R.; Scholl, A. *J. Am. Chem. Soc.* **2003**, *125*, 8302.

(31) LeMieux, M. C.; Peleshanko, S.; Anderson, K. D.; Tsukruk, V. V. *Langmuir* **2007**, *23*, 265.

(32) Minko, S.; Müller, M.; Motornov, M.; Nitschke, M.; Grundke, K.; Stamm, M. *J. Am. Chem. Soc.* **2003**, *125*, 3896.

(33) Julthongpipit, D.; Lin, Y.; Teng, J.; Zubarev, E. R.; Tsukruk, V. V. *Langmuir* **2003**, *19*, 7832.

(34) Julthongpipit, D.; Lin, Y.; Teng, J.; Zubarev, E. R.; Tsukruk, V. V. *J. Am. Chem. Soc.* **2003**, *125*, 15912.

(35) Zhang, Q.; Archer, L. A. *Langmuir* **2006**, *22*, 717.

(36) Furey, J. M. In *The Biomedical Engineering Handbook*, 2nd ed.; Bronzino, J. D., Ed.; CRC Press LLC: Boca Raton, FL, 2000; Vol. 1, pp 21-1 to 21-25.

(37) Milner, S. T. *Science* **1991**, *251*, 905.

(38) de Gennes, P. G. *Macromolecules* **1980**, *13*, 1069.

(39) de Gennes, P. G. *Adv. Colloid Interface Sci.* **1987**, *17*, 189.

(40) Müller, M. T.; Yan, X.; Lee, S.; Perry, S. S.; Spencer, N. D. *Macromolecules* **2005**, *38*, 5706.

Recently, it has been demonstrated that metal oxide surfaces coated with a molecularly thin layer of poly(L-lysine)-graft-poly(ethyleneglycol) (PLL-*g*-PEG) brushes exhibited reduced friction at the nano- and macroscale levels.<sup>40–43</sup> More importantly, the lubricity of these *hydrophilic* films was strongly dependent on solvent quality, in both single and binary solvent systems, being reduced as the nonpolar character of the solvent increased.<sup>40,41</sup> The higher friction was correlated with the collapsed conformation of the polymer brush in a poor solvent environment.

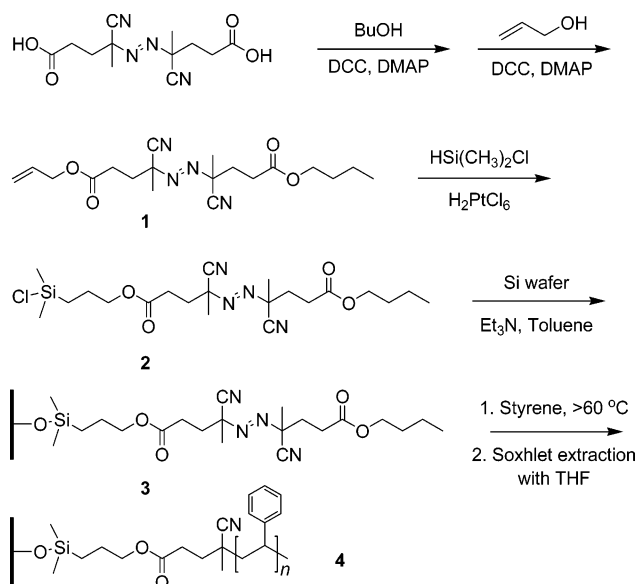
This paper aims to complement these results by demonstrating a similar general behavior: the increase in lubricity of a *hydrophobic* brush in a *nonpolar* solvent environment. Whereas preformed PLL-*g*-PEG “bottle-brushes” were attached to oxide surfaces via electrostatic interactions by regulating the pH, here, polystyrene (PS) brushes were covalently attached to oxide passivated silicon wafers by direct polymerization of styrene on its surface.

Normal and shear forces have been previously measured with the surface force apparatus (SFA) between mica surfaces bearing preformed polystyrene adsorbed via a terminal zwitterionic group.<sup>6,44,45</sup> Normal forces became repulsive at higher polymer adsorption and at higher shear rates,<sup>44,45</sup> while shear forces remained extremely weak in good solvent over a wide range of velocities.<sup>6</sup>

Higher polymer brush densities can be achieved by the direct polymerization from the surface rather than attaching preformed polymers.<sup>1,46,47</sup> In the past, this has been realized through the self-assembly of initiators on the surface through (a) functionalizing the surface with groups that initiators can then attach to,<sup>48</sup> (b) synthesis of asymmetric initiators with an anchoring functionality,<sup>46,47,49</sup> or (c) a combination of both.<sup>50</sup> This work takes the route of asymmetrically modifying the available 4,4'-azobis(4-cyanovaleic acid), an AIBN-type initiator, with a double bond functionality that can then be coupled with a monochlorosilane. This provides a path to tether it onto the silicon oxide substrate by a condensation reaction with the terminal hydroxy groups. The mechanism and kinetics of the surface initiated free-radical polymerization (SIP) of styrene has been extensively studied.<sup>47</sup> SIP, in general, represents a versatile method of tailoring the lubricity of surfaces with a wide range of polymer–solvent systems.

Nanoscale friction force measurements were performed on these systems via atomic force microscopy (AFM), employing a 5  $\mu\text{m}$  SiO<sub>2</sub> colloidal probe while systematically varying the environment from good (toluene) to poor (2-propanol and *n*-butanol) solvents, with respect to the molecular composition of the polystyrene brush. The relative solvent uptake and viscoelastic response of the brush system were monitored with a quartz crystal microbalance (QCM) for the solvent series.

### Scheme 1. Preparation of a PS Brush on a Si Wafer Surface



## 2. Experimental Section

**2.1. Synthesis of Azochlorosilane Initiator.** The surface attached free radical initiator was prepared by asymmetrically modifying 4,4'-azobis(4-cyanovaleic acid) through the consecutive Steglich esterifications of the carboxy moieties,<sup>50</sup> first with *n*-butanol, followed by allyl alcohol (Scheme 1).

A solution was prepared consisting of 5.60 g (20 mmol) of the azo initiator, 75 mg of 4-(dimethylamino)pyridine (DMAP), and 1.48 g (20 mmol) of *n*-butanol in about 40 mL of dry, distilled tetrahydrofuran (THF) and then cooled to ice bath temperature. To this, a 15 mL THF solution of 4.12 g (20 mmol) of *N,N'*-dicyclohexylcarbodiimide (DCC) was slowly dripped and then stirred for 3 h at room temperature. The urea byproduct was removed by vacuum filtration through a membrane filter with a 0.10  $\mu\text{m}$  cutoff, and the filtrate was reduced through the removal of THF by rotavap below 40 °C. This was then added to water, extracted with dichloromethane, washed with brine solution, and dried over magnesium sulfate. The dichloromethane was removed by rotavap below 40 °C, and the residue was further dried under vacuum overnight. This procedure should give a statistical product (actual yield 78%) in which one carboxy moiety is capped with a butyl group. Without further purifications, this crude product was used in the next step where the remaining carboxy moiety was esterified with an equimolar amount of allyl alcohol by the same DCC/DMAP procedure to yield product **1** (actual yield 92%), introducing a double bond functionality to the azo initiator. This transformation was indicated by the appearance of vinyl <sup>1</sup>H NMR shifts at 5.2, 5.3, and 5.9 ppm. The <sup>1</sup>H NMR data were acquired in CDCl<sub>3</sub>, on the General Electric QE-300 spectrometer, and processed using NUTS software (Acorn NMR, Inc., CA).

This vinyl species allowed the addition of a chlorosilane group to the azo initiator by hydrosilylation,<sup>46,51</sup> which then provided an anchor to the oxide layer on a silicon wafer. Since chlorosilanes are very reactive with moisture, all reactions were carried out in dry apparatus under a nitrogen atmosphere. A total of 5 mL of dimethylmonochlorosilane and a catalytic amount of hexachloroplatinic acid was added to product **1**, which had been previously vacuum-dried overnight. The mixture was refluxed at 35 °C for 3 h and then left to stir at room temperature overnight. Excess dimethylmonochlorosilane was removed by rotavap below 40 °C. The remaining product **2** was dissolved in a small amount of dry, distilled toluene and then quickly filtered through magnesium sulfate to remove both trace moisture and platinum catalyst. The disap-

(41) Müller, M. T.; Yan, X.; Lee, S.; Perry, S. S.; Spencer, N. D. *Macromolecules* **2005**, *38*, 3861.

(42) Yan, X.; Perry, S. S.; Spencer, N. D.; Pache, S.; De Paul, S. M.; Textor, M.; Lim, M. S. *Langmuir* **2004**, *20*, 423.

(43) Spencer, N. D.; Perry, S. S.; Lee, S.; Müller, M.; Pache, S.; De Paul, S. M.; Textor, M.; Yan, X.; Lim, M. S. In *Tribological Research and Design for Engineering Systems*, Proceedings of the 29th Leeds-Lyon Symposium (Tribology and Interface Engineering); Dowson, D., Lubrecht, A.A., Dalmaz, D., Priest, M., Eds.; Elsevier Science: London, 2003; pp 411–416.

(44) Taunton, H. J.; Toprakcioglu, C.; Fetters, L. J.; Klein, J. *Nature* **1988**, *332*, 712.

(45) Klein, J.; Perahia, D.; Warburg, S. *Nature* **1991**, *352*, 143.

(46) Prucker, O.; Rühle, J. *Macromolecules* **1998**, *31*, 592.

(47) Prucker, O.; Rühle, J. *Macromolecules* **1998**, *31*, 602.

(48) Tsubokawa, N.; Kogure, A.; Maruyama, K.; Sone, Y.; Shimomura, M. *Polym. J.* **1990**, *22*, 827.

(49) Parvole, J.; Laruelle, G.; Guimon, C.; Francois, J.; Billon, L. *Macromol. Rapid Commun.* **2003**, *24*, 1074.

(50) Fan, X.; Xia, C.; Fulghum, T.; Park, M.; Locklin, J.; Advincula, R. C. *Langmuir* **2003**, *19*, 916.

(51) Brook, M. A.; Neuy, A. *J. Org. Chem.* **1990**, *55*, 3609.

pearance of the vinyl  $^1\text{H}$  NMR shifts and the appearance of methyl proton shifts on Si around 0 ppm indicated the formation of **2**.

**2.2. Surface Initiated Polymerization (SIP) of Styrene.** Silicon wafers, cut into small strips, were cleaned before use as follows: sonication in a dilute cleaning solution (Fisherbrand Ultrasonic Cleaning Solution, Fisher Scientific) for 15 min, followed by ultrapure water (18.2 M $\Omega$ ) for 5 min, soaking in piranha solution (70:30 H $_2$ SO $_4$ /30% H $_2$ O $_2$ ) for 30 min, and washing and sonication in ultrapure water for 10 min. (**Caution!** Piranha solution is highly corrosive and oxidizing!) After drying in the oven, the silicon wafer was cleaned in an oxygen plasma for 2 min and placed flat at the bottom of a septum-sealed vial that was purged with nitrogen gas. Into this vial, dry, distilled toluene and 0.1 mL each of triethylamine and the azochlorosilane **2** toluene solution were added. The reaction was allowed to run overnight, after which the azo-modified silicon wafer **3** was washed thoroughly with methanol.

This azo-modified silicon wafer was placed in a reaction vessel that was charged with 10 mL of styrene monomer from which the inhibitor was previously removed with basic alumina. The system was degassed to remove oxygen by four successive freeze–pump–thaw cycles and then allowed to polymerize with stirring at 60–75 °C for 43 h. The reaction was terminated by exposure to air. The PS-modified silicon wafer **4** was washed by Soxhlet extraction in THF for 44 h to remove any free polymer.

A similar procedure was employed to graft polystyrene onto a QCM quartz crystal with a SiO $_2$ -sputtered gold electrode face (Maxtek, Inc., CA). The quartz crystal was washed with 2-propanol and then plasma cleaned under oxygen for 200 s before use. The styrene monomer was degassed separately from the azo-modified quartz crystal to prevent it from fracturing under the freeze–pump–thaw regime. Finally, as the active area on the quartz crystal consists of a complex multilayer (Ti/Au/Ti/SiO $_2$ ), a separate azo-modified silicon wafer was included in the reaction vessel to carry out concurrent polymerization for thickness measurements. Total reaction time was 24 h, followed by 40 h of Soxhlet extraction in THF.

**2.3. Characterization of the Surface Modifications.** The surface modifications on the silicon wafer were monitored by ellipsometry and X-ray photoelectron spectroscopy (XPS). Thickness measurements were performed on the Multiskop system (Optrel GmbH, Germany) equipped with a 632.8 nm He–Ne laser source at an incident angle of 60°. The ellipsometric parameters  $\Delta$  and  $\Psi$  were recorded on at least three areas on the sample. Together with the material's refractive index ( $n$ ) and extinction coefficient ( $k$ ), these values were used in a layer model to calculate an average film thickness.

Analysis of the surface elemental composition was performed using a PHI model 5700 X-ray photoelectron spectrometer equipped with a monochromatic Al K $\alpha$  X-ray source ( $h\nu = 1486.6$  eV, 350.0 W) incident at 90° relative to the axis of a hemispherical energy analyzer. The spectrometer was operated at low (survey) resolution with 187.85 eV pass energy and at high resolution with 23.50 eV pass energy, with a photoelectron takeoff angle of 45° from the surface and an analyzer spot diameter of 1.1 mm. The survey spectra were collected from 0 to 1400 eV, and the high-resolution spectrum was obtained in the C 1s, O 1s, and N 1s regions. The O 1s peak of the SiO $_2$  signal (533 eV) was used as the binding energy reference. All spectra were obtained at room temperature and at a base pressure of about 10 $^{-8}$  Torr. Atomic concentrations were estimated from peak areas and published instrumental sensitivity factors.<sup>52</sup>

**2.4. AFM Measurements.** Friction force measurements were performed utilizing a home-built AFM scan head equipped with a liquid cell/tip holder (Digital Instruments, CA), controlled by AFM100/STM100 feedback electronics and SPM32 software (RHK Technology, Inc., MI). The microscope employs a single tube piezo to move the sample relative to a fixed tip position. Reflection of a laser beam from the back of the cantilever is detected by a four-quadrant photodiode. Details of this assembly have been reported elsewhere.<sup>53,54</sup>

The tip consisted of a 5  $\mu\text{m}$  silica colloidal sphere affixed to a cantilever (Novascan Technologies, IA); this sphere surface served as the counterface to the PS brush-modified silicon wafer surface. The tip was used as received, with the spherical shape of the probe validated by optical microscopy. Its surface roughness was not determined; however, valid comparisons of friction measurements have been made possible with the use of the same tip on the same sample, with only the solvents exchanged *in situ*.

Kinetic friction was measured by monitoring the lateral deflection of the cantilever as a function of tip position during sliding and loading/unloading. This was implemented by rastering the sample in a line-scan mode as the load was ramped up and then down, while simultaneously recording both normal and frictional forces.

A single cantilever assembly was employed for all of the measurements reported in this study. Normal loads were determined from the cantilever's nominal spring constant ( $k = 0.58$  N/m, manufacturer's reported value) and direct measurements of sample displacement. Such a cantilever/microsphere assembly would exert a pressure of 95.6 MPa at an applied load of 20 nN on a silicon surface, assuming a Hertzian contact of  $\sim 210$  nm $^2$ .

The friction force response was taken to be the half-difference of the average lateral deflection signal on the photodetector of the forward and reverse traces, that is, a friction loop. Lateral forces were calibrated by sliding the tip at given normal load set-points across a silicon grating with known slopes (TGF11, MikroMasch, Spain). Details of this procedure have been reported elsewhere.<sup>55</sup>

Measurements employed a scan rate of  $\sim 1400$  nm/s over a distance of 100 nm. The reported friction data represent the increasing normal load ramp, with maximum applied loads of less than 60 nN to avoid tip and sample wear. At least three acquisitions over several regions on the sample were averaged, with offset tip positions falling within an area of 50 nm $^2$ . Solvents were exchanged in the order of toluene, 2-propanol, and *n*-butanol by transferring aliquots in and out of the liquid cell using two 5 mL syringes.

Topographic images for surface roughness analysis were obtained in AC mode using an MFP-3D atomic force microscope (Asylum Research, CA), employing a tip cantilever with a nominal resonance frequency of 70 kHz (AC240TS, Olympus, Japan). Images were collected at 1  $\mu\text{m}^2$  scan sizes, at scan rates of 0.80 Hz, over a 10  $\mu\text{m}^2$  sampling area.

**2.5. QCM Measurements.** The QCM system used for solvent uptake measurements was assembled from a SA250B-1 Network Analyzer and test fixture (Saunders & Associates, Inc., AZ), a liquid flow cell (Maxtek, Inc., CA), and QTZ control software (Resonant Probes GmbH, Germany). The resonators consisted of AT-cut quartz crystals, also from Maxtek, Inc., with silica-sputtered gold electrodes and a fundamental resonance frequency of 5 MHz.

Solvent exchange experiments were performed on both blank and PS brush-modified quartz crystals. The blank quartz crystal was cleaned prior to use by sonication in acetone, 2-propanol, and ultrapure water for 5 min each. It was then plasma cleaned for 1 min under O $_2$ /H $_2$ O $_2$  process gas. The PS brush-modified quartz crystal was simply washed with 2-propanol and then dried in air prior to use. The quartz crystals were installed in the flow cell 1 day prior to making measurements to allow for the stress-relaxation of the Viton O-ring. Data were collected in air for 100 min prior to the first solvent injection to ensure the stabilization of the system. Data were then collected in 10 min intervals between each solvent exchange. The reported frequency and bandwidth shifts represent the average of data collected over a period of 5 min.

### 3. Results and Discussion

**3.1. Surface Characterization by XPS Analysis.** Covalent grafting of PS onto silicon wafers was followed by XPS analysis. The inset in Figure 1 displays the XPS spectra after cleaning

(52) Moulder, J. F.; Stickle, W. F.; Sobol, P. E.; Bomben, K. D. *Handbook of X-Ray Photoelectron Spectroscopy*; Perkin-Elmer: Waltham, MA, 1995.

(53) Perry, S. S. *MRS Bull.* **2004**, 29, 478.

(54) Perry, S. S.; Somorjai, G. A.; Mate, C. M.; White, R. L. *Tribol. Lett.* **1995**, 1, 233.

(55) Ogletree, D. F.; Carpick, R. W.; Salmeron, M. *Rev. Sci. Instrum.* **1996**, 67, 3298.

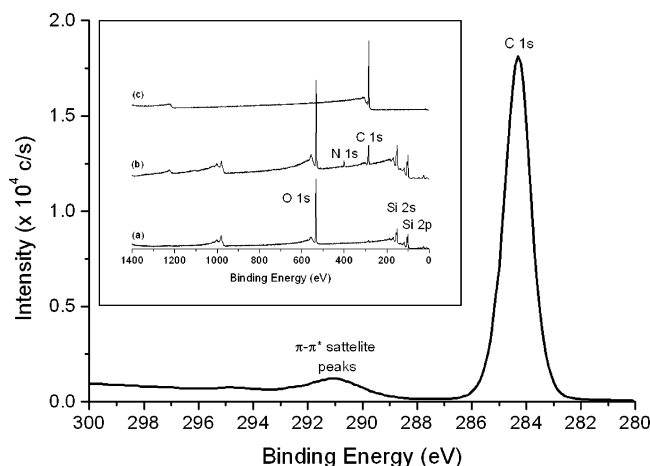


**Figure 1.** High-resolution X-ray photoelectron spectrum of a silicon wafer after surface initiated polymerization of styrene. The  $\pi-\pi^*$  shakeup satellite peak near the C 1s region appears due to the styrene aromatic ring. Inset: survey spectra of silicon wafers after (a) cleaning with  $O_2$  plasma, (b) grafting of azo initiator, and (c) surface initiated polymerization of styrene.

with oxygen plasma, after grafting of the azo initiator, and finally after the surface initiated polymerization of styrene.

The XPS analysis on the clean silicon wafer was performed immediately following plasma cleaning. The survey spectrum (Figure 1, inset (a)) includes peaks characteristic of silicon and oxygen. A small amount of adventitious carbon is also present.

After the self-assembly of the azo initiator on the clean silicon wafer, characteristic peaks in the survey spectrum (Figure 1, inset (b)) for nitrogen (N 1s) and carbon (C 1s) appeared at 400 and 286 eV, respectively. The high-resolution spectrum of the N 1s region showed two overlapping peaks at 400.0 and 401.5 eV, assigned to the nitrogens of the cyano and azo groups,<sup>56</sup> respectively. The relative atomic concentrations of carbon and nitrogen were calculated by integration of the peak areas, with intensities normalized according to the particular element's sensitivity. The observed C/N atomic concentration ratio (84:16) correlates well with the grafted azo initiator **3** composition, that is, 21 C atoms to 4 N atoms. In some measurements, 87% C was observed, due most probably to the presence of adventitious carbon. Oxygen in the azo initiator was not included in this analysis, as its intensity was convoluted with the large background signal of  $SiO_2$ .

After grafting polystyrene, the survey spectrum (Figure 1, inset (c)) shows the absence of the characteristic silicon and oxygen peaks from  $SiO_2$  and of any nitrogen peaks from unreacted initiator or that part that remains attached to the silicon wafer after its fragmentation. High resolution analysis of the C 1s region (280–300 eV) revealed a large peak at 284.2 eV characteristic of a hydrocarbon system as well as a small satellite peak at 291.1 eV assigned to a  $\pi-\pi^*$  shakeup, indicative of the styrene aromatic ring.<sup>57</sup>

**3.2. Ellipsometric Film Thickness Measurements.** Ellipsometric measurements were performed after each stage in the modification of the silicon wafer to provide data for the layer model.<sup>58</sup> First, the average  $SiO_2$  layer (of six different samples) was calculated to be  $14 \pm 3 \text{ \AA}$ . The thickness of the azo initiator

film was then evaluated using a two-layer model. Since the refractive index of this compound is not known, the one for (3-aminopropyl)trimethoxysilane ( $n = 1.424$ ), commonly used in functionalizing silica surfaces, was used as a working value. The estimated azo initiator thickness (of six different samples) was calculated to be  $11 \pm 4 \text{ \AA}$ . Finally, the thickness of the PS film was evaluated using a three-layer model and  $n = 1.591$ . The sample used for AFM friction measurements was calculated to have an average dry thickness of  $117.6 \pm 0.6 \text{ nm}$ , measured at 5 different areas on each of two different samples.

The active area on the QCM crystal consisted of a complex multilayer of quartz/Ti/Au/Ti/ $SiO_2$ , and as we did not have information about the thicknesses of the underlying layers, it was not possible to directly track modifications by ellipsometric modeling. The thickness of the PS film on the QCM crystal was therefore estimated from a silicon sample on which PS was concurrently polymerized in the same vessel. The average value was  $30 \pm 9 \text{ nm}$ , measured at 5 different areas on the sample, being less than that of the AFM sample as a result of shorter reaction time. However, differences in the roughness, or root-mean-square (rms) height, of the silica layer on the Si wafer ( $0.22 \pm 0.02 \text{ nm}$ ) and on the QCM crystal ( $1.78 \pm 0.08 \text{ nm}$ ) may also contribute to discrepancies in the estimated PS thickness values. The rms heights are averages taken from  $1 \mu m^2$  scan sizes at different locations within a  $10 \mu m^2$  area.

### 3.3. QCM Solvent Uptake and Dissipation Monitoring.

When considered as an acoustic reflectometer, a quartz crystal resonator may be used to probe loads at the interface from the phase shift in the total reflection amplitude.<sup>59,60</sup> The complex frequency shift ( $\Delta f^*$ ) takes account of both the elastic and dissipative interactions of the quartz crystal with its environment.

$$\frac{\Delta f^*}{f} = \frac{\Delta f + i\Delta\Gamma}{f} = \frac{i}{\pi Z_q} Z_s \quad (1)$$

Here,  $\Delta\Gamma$  is the bandwidth shift, related to dissipation ( $D = 2\Gamma/f$ ),  $Z_q$  is the acoustic impedance of an AT-cut quartz, and  $Z_s$  is the load impedance at the quartz-sample interface. In the Sauerbrey limit, that is, a thin rigid film in air or vacuum, there is no bandwidth shift, and the fractional shift in frequency is simply proportional to the mass loading on the quartz crystal.<sup>61</sup>

Under liquid, the load impedance is simply the acoustic impedance of the liquid, which depends on both its density and viscosity. The general Kanazawa relation predicts that, under a purely viscous load, the frequency shift is simply the negative of the bandwidth shift.<sup>61,62</sup> In other words, since there is no mass loading, the frequency shift is only attributable to dissipative interaction with a Newtonian fluid. For a viscoelastic film in contact with a liquid, the complex frequency shift includes both a Kanazawa term and a Sauerbrey term.<sup>59,61</sup> In the thin film limit, the frequency and bandwidth shifts are the sums of the Kanazawa and Sauerbrey contributions.

In the present study of PS brushes under varying solvent environments, measurements were performed on a blank crystal in addition to the PS-modified quartz crystal. In the blank, there was no mass loading, and therefore, the frequency shift approximates the bandwidth shift but with opposite sign (Table 1). However, for the PS-modified quartz crystal, mass loading due to the solvent uptake in the polymer produced different readings. The Sauerbrey contribution can be extracted from the

(56) McCoy, K.; Hess, D. W.; Henderson, C. L.; Tolbert, L. M. *J. Vac. Sci. Technol., B* **2004**, *22*, 3503.

(57) Briggs, D. *Surface Analysis of Polymers by XPS and Static SIMS*; Cambridge University Press: Cambridge, U.K., 1993.

(58) Minko, S.; Patil, S.; Datsyuk, V.; Simon, F.; Eichhorn, K.; Motornov, M.; Usov, D.; Tokarev, I.; Stamm, M. *Langmuir* **2002**, *18*, 289.

(59) Johannsmann, D. *Macromol. Chem. Phys.* **1999**, *200*, 501.

(60) Wolff, O.; Seydel, E.; Johannsmann, D. *Faraday Discuss.* **1997**, *107*, 91.

(61) Goubaidouline, I.; Reuber, J.; Merz, F.; Johannsmann, D. *J. Appl. Phys.* **2005**, *98*, 014305.

(62) Kanazawa, K. K.; Gordon, J. G., II. *Anal. Chim. Acta* **1985**, *175*, 99.

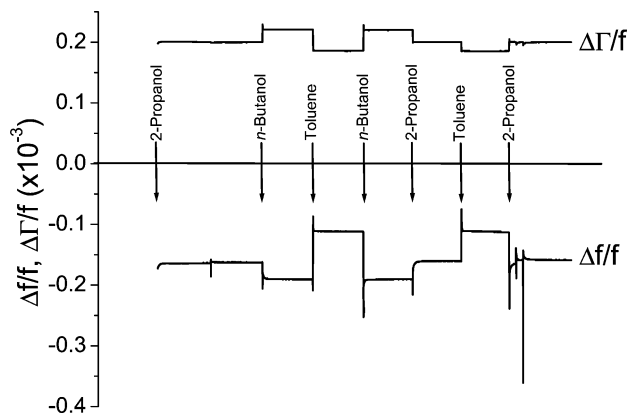


**Figure 2.** Fractional shifts in the frequency and bandwidth of a PS brush-modified quartz crystal resonator under 2-propanol, *n*-butanol, and toluene.

**Table 1. Normalized Frequency and Bandwidth Shifts of PS Modified and Blank Quartz Crystals under Various Solvent Environments. Sauerbrey Mass and Dissipation are Calculated from the Difference**

solvent	average $\Delta f/f (\times 10^{-3})$			Sauerbrey mass ( $\mu\text{g}/\text{cm}^2$ )
	PS modified	blank	difference	
2-propanol	-0.1615	-0.1551	-0.0074	0.559
<i>n</i> -butanol	-0.1904	-0.1759	-0.0145	1.276
toluene	-0.1120	-0.0904	-0.0217	1.910

solvent	average $\Delta\Gamma/f (\times 10^{-3})$			dissipation ( $\times 10^{-3}$ )
	PS modified	blank	difference	
2-propanol	0.2000	0.1959	0.0041	0.0067
<i>n</i> -butanol	0.2205	0.2198	0.0006	-0.0002
toluene	0.1855	0.1101	0.0754	0.1500

observed frequency shift by the subtraction of the Kanazawa contribution as determined from the blank.

$$\Delta f_{\text{Sauerbrey}} = \Delta f_{\text{observed}} - \Delta f_{\text{Kanazawa}} \quad (2)$$

A comparison of the blank and the PS-modified  $\Delta f/f$  data shows only small differences under 2-propanol and *n*-butanol. Under toluene, however, the PS-modified quartz crystal exhibited a considerably more negative frequency shift. Using the Sauerbrey relation, areal mass densities representing the solvent uptake in the polymer brush were estimated from the differences in the frequency shifts between the PS-modified quartz crystal ( $\Delta f_{\text{observed}}$ ) and the blank ( $\Delta f_{\text{Kanazawa}}$ ). The PS brush shows a higher relative solvent uptake in toluene compared to the alcohols.

A comparison of the  $\Delta\Gamma/f$  data reveals that, under 2-propanol and *n*-butanol, the PS-modified quartz crystal closely follows the Kanazawa condition, as in the blank. Under toluene, however, the PS-modified crystal considerably departs from this condition; that is, a higher bandwidth shift is observed than what is expected in the Kanazawa regime (Figure 2). This is attributed to a change in the viscoelastic behavior of the polymer film, becoming more lossy or plasticized as it swells upon solvation. These observations are consistent with the swelling behavior observed in the AFM force–displacement plots and the high lubricity of polymer brushes under good solvents.

**3.4. AFM Force Measurements.** With the PS-modified silicon surface under a toluene solution, friction was measured by rastering the sample in a direction perpendicular to the cantilever axis while first increasing and then decreasing the normal load. Both the normal and lateral deflections of the cantilever were

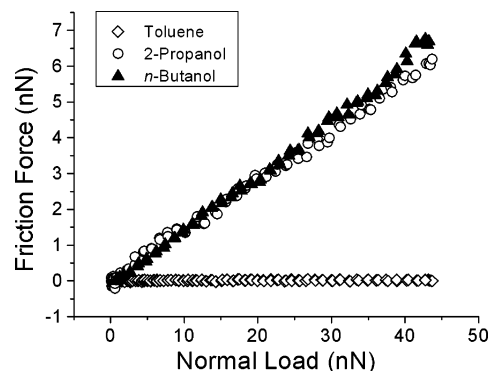


**Figure 3.** Friction force versus normal load between a  $5 \mu\text{m}$   $\text{SiO}_2$  probe and a PS brush-modified (117.6 nm thick) Si wafer, under 2-propanol, *n*-butanol, and toluene. The plots are representative of at least five measurements using the same tip at different areas of the sample for each solvent.

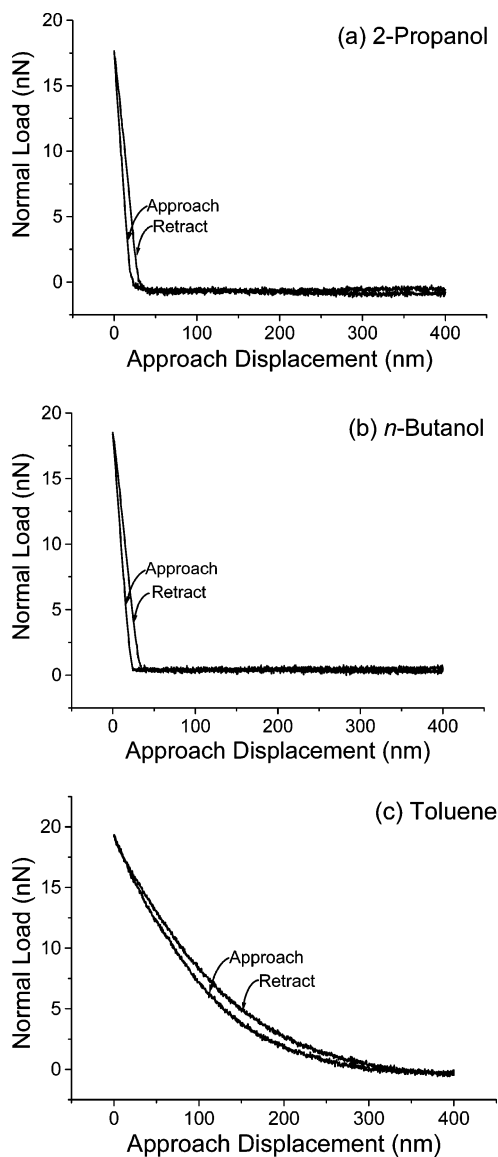
simultaneously recorded, with friction data consisting of the lateral force response as a function of normal load.

Figure 3 shows representative friction force measurements for two poor solvents (2-propanol and *n*-butanol) and a good solvent (toluene) of polystyrene. The solvents were exchanged in the order of toluene, 2-propanol, and *n*-butanol. Valid comparison of the data was enabled through the use of the same tip throughout, at the same modest normal force range ( $<60$  nN), and exchange of solvents *in situ* so that the tip probed the same small area. Under 2-propanol and *n*-butanol, the slopes, which represent coefficients of friction, are both around 0.16, with mean errors of  $2 \times 10^{-3}$ , averaged from six different regions. Under toluene, the plot illustrates a vanishingly low friction coefficient between the tip and PS brush, 3 orders of magnitude lower than those measured in 2-propanol and *n*-butanol, with a mean error of  $3 \times 10^{-4}$ . These trends were likewise obtained with different PS brush samples.

Topographic images (see the Supporting Information) also reveal changes in surface roughness under the different solvent environments studied. In air, the rms height of the PS brush is  $0.8 \pm 0.3$  nm; this decreased to  $0.19 \pm 0.05$  nm in toluene and increased to  $5 \pm 2$  nm in 2-propanol. The rms height averages were calculated from  $1 \mu\text{m}^2$  scan sizes obtained in different locations over a  $10 \mu\text{m}^2$  area. Although these changes are consistent with the observed friction response, quantitative correlation of these roughness and friction values is complicated by the 3 to 4 orders of magnitude difference in the sampling frequency of the two measurement approaches.

Normal force versus tip displacement plots were also obtained at single points across the surface and in different solvents. Figure 4 shows the approach and retract traces of the silica colloidal probe toward the PS brush sample under toluene, 2-propanol, and *n*-butanol. The approach and retract curves under toluene demonstrate the elastic character of these brushes under this solvent. Slight differences in normal forces in the approach and retract traces for a given displacement arise as a result of piezo hysteresis.

Two things are observed from these data: first, the contact point between the tip and the sample occurs at a much greater distance from the Si substrate under toluene as compared to under the alcohol solvents. This is clear evidence that the polymer brush exists in a stretched conformation under toluene and, conversely, in a relatively collapsed state under the alcohols. Contact here is taken to be the point of departure from an equilibrium cantilever deflection in the force–displacement plot. Second, the shapes of the plots differ significantly, indicating



**Figure 4.** AFM force versus displacement plots of a  $5\ \mu\text{m}$   $\text{SiO}_2$  probe on a PS brush-modified ( $117.6\ \text{nm}$  thick) Si wafer under (a) 2-propanol, (b) *n*-butanol, and (c) toluene.

substantial differences in the contact mechanics of the brush under different solvents. The tip encounters a harder surface when pushing against the PS brush under alcohol and a softer surface when pushing against the same under toluene. Under toluene, a good solvent for polystyrene, the polymer brush is heavily solvated and assumes a stretched conformation; upon compression by the application of load, the solvent is slowly exuded from the polymer brush, a process that is reversed upon retraction of the tip.

**3.5. Discussion.** The nanometer scale measurements of interfacial friction for the contact of a colloidal  $\text{SiO}_2$  probe and polystyrene brushes clearly demonstrate a strong dependence of friction on the solvent environment. This dependence is understood in terms of the influence of the solvent environment on the conformational state of the brush, a claim consistently supported by the complementary QCM and AFM force displacement data. Together, these measurements portray the significant swelling of the brush structure upon exposure to a toluene solvent and the corresponding collapse when exposed to 2-propanol and *n*-butanol solvents. These molecular scale conformational changes result from the respective intermolecular interactions between the polymer brush and solvent molecules, which can be

rationalized through a three-component Hansen solubility parameter model.<sup>40,63,64</sup> This approach is commonly used to predict the solubility of a polymer in a solvent.<sup>65</sup>

Solubility parameters effectively describe the cohesive energy of a solvent system and can be expressed in terms of the Hansen dispersion, polar, and hydrogen-bonding components of the net interaction energy. These can be used to derive a single value  $H$ , the ratio of cohesive energy densities, which indicates a polymer's relative solubility in a given set of solvents.  $H$  represents the ratio of the overall difference in the Hansen parameters between the solvent and polymer and the maximum difference tolerated by the polymer for solution to occur. It can be used to estimate the Flory interaction parameter ( $\chi_{12}$ ) for higher molecular weight polymers.<sup>63</sup>

The values of  $H$  for the solvents employed in this study decrease in the order of 2-propanol ( $H = 1.66$ ), *n*-butanol ( $H = 1.52$ ), and toluene ( $H = 0.42$ ), where a value of less than 1 represents high affinity with polystyrene. Overall, they portray greater intermolecular attractions between a *nonpolar* solvent (toluene) and a *hydrophobic* polymer such as polystyrene, relative to the latter's interaction with *polar* solvents (2-propanol, *n*-butanol). These values are consistent with the measured trends in solvent uptake and brush swelling, where solvent–polymer interactions drive the swelling of the brush and conformational changes depicted in AFM force–displacement curves. As described in our previous work considering the solvation of PLL-*g*-PEG in a range of solvents,<sup>40,41</sup> we conclude that such conformations and favorable solvent–brush interactions represent the necessary criteria for the low friction measured at highly solvated polymer brush surfaces. In light of the results of prior studies,<sup>40,41</sup> the present report of low friction measured for a *hydrophobic* brush system in the presence of a *nonpolar* solvent clearly supports the general description of brush lubricity in these solvation terms.

#### 4. Conclusion

Polystyrene brushes were prepared on oxide passivated silicon surfaces by surface initiated free-radical polymerization and investigated in a range of solvent environments. It was observed that the PS brush exhibited a relatively higher solvent uptake in toluene compared to 2-propanol and *n*-butanol. In turn, PS brushes exhibited vanishingly low friction in toluene, a good solvent, versus 2-propanol and *n*-butanol. In force–displacement plots, contact was observed at relatively greater tip–substrate separations under toluene compared to the alcohols, supporting the idea of brush swelling. These studies support the reliance of the frictional properties of polymer brush-modified interfaces on the quality of the solvent environment and the resulting conformation of the brush structure.

**Acknowledgment.** The authors acknowledge the Air Force Office of Scientific Research (AFOSR) for support of this research. The authors also acknowledge the thoughtful input of Prof. Nic Spencer and Dr. Seunghwan Lee of ETH-Zurich.

**Supporting Information Available:** Topographic images of PS brush-modified SI wafers in air and under toluene and 2-propanol. This material is available free of charge via the Internet at <http://pubs.acs.org>.

LA701272A

(63) Hansen, C. M. *Hansen Solubility Parameters: A User's Handbook*; CRC Press: Boca Raton, FL, 2000.

(64) Barton, A. F. M. *Handbook of Polymer-Liquid Interaction Parameters and Solubility Parameters*, 2nd ed.; CRC Press: Boca Raton, FL, 1991; pp 11–15.

(65) Zhao, L. Y.; Choi, P. *Polymer* **2004**, *45*, 1349.